Nano Energy 73 (2020) 104744

Contents lists available at ScienceDirect

Nano Energy

journal homepage: http://www.elsevier.com/locate/nanoen

High-performance Sb-doped p-ZnO NW films for self-powered piezoelectric strain sensors

Zhihao Huo [a,b,1], Xiandi Wang [a,b,1], Yufei Zhang [a,b,1], Bensong Wan [a,c], Wenqiang Wu [a], Jianguo Xi [a], Zheng Yang [a], Guofeng Hu [a,c], Xiangyu Li [a,b], Caofeng Pan [a,b,c,d,*]

[a] CAS Center for Excellence in Nanoscience, Beijing Key Laboratory of Micro-nano Energy and Sensor, Beijing Institute of Nanoenergy and Nanosystems, Chinese Academy of Sciences, Beijing, 100083, PR China
[b] School of Nanoscience and Technology, University of Chinese Academy of Sciences, Beijing, 100049, PR China
[c] Center on Nanoenergy Research, School of Physical Science and Technology, Guangxi University, Nanning, Guangxi, 530004, PR China
[d] College of Optoelectronic Engineering, Shenzhen University, Shenzhen, 518060, China

ARTICLE INFO

Keywords:
Sb-doped p-ZnO NW films
MIS junction
Schottky devices
Piezotronic effect
PENGs

ABSTRACT

Novel wide-bandgap piezoelectric semiconductor materials, with wurtzite structure, set a great impetus to research, which outreach the promising applications in optoelectronic devices, wearable electronic devices and medical monitoring systems. Here, we studied the piezotronic effect of p-ZnO NW films under strain which were suitable for self-powered tactile sensors. Typically, the doping level was 2×10^{17} cm^{-3} at the 2% Sb doping in solution. Based on different devices design, it was verified that the piezoelectric charges induced by applied strain could significantly affect the charge carrier separation and transport at the interface/junction. For p-ZnO NW thin film devices, the negative piezoelectric charge reduces Schottky barrier height, while the positive piezoelectric charge increases it. Self-powered strain sensors were then developed based on the changes of piezoelectric potential under different strain, which have a potential candidate for applications in man-machine interaction interface and biomedical sciences.

1. Introduction

Blooming of nanomaterials in the novel third-generation semiconductor that underpin the information industry, boost the development of cutting-edge technological revolutions and emerging industries [1–3]. Among them, ZnO with the direct bandgap and exciton binding energy of up to 60 meV has been widely applied in solar cells [4–6], light-emitting diodes (LEDs) [7–9], and strain sensors [10–12]. In addition, ZnO exhibits excellent piezoelectric properties under external strain due to non-central symmetric crystal structure [13,14], making it possible for flexible and bio-driven electronics that employ mechanical stimuli directly to generate digital signals, such as piezoelectric nanogenerators (PENGs) [15,16] and self-powered devices [17–19]. However, most of the aforementioned devices were fabricated using n-type ZnO, and there are few studies about the piezoelectric effect of p-type ZnO films and its application in strain sensors.

Several excellent studies and theoretical reports on p-type ZnO have aroused intensive attention. Nevertheless, the p-type ZnO is still a bottleneck and research hotspot, which restricts the application of ZnO-based devices, even if various growth techniques of p-ZnO with different dopants have been demonstrated [20–23]. In 2007, Wang first developed piezotronics effect that piezoelectric potential induced by strain can regulate the carrier transport characteristic in non-central symmetrical semiconductors [24]. Subsequently, many pioneering works were reported, such as piezotronic transistors [25,26], logic devices [27], gas and humidity sensors [28,29] and self-powered devices [30–32]. It was noteworthy that an array of over 20 000 piezotronic LEDs-based pressure sensors have been reported for tactile imaging at a resolution of 2.7 μm with a corresponding pixel density of 6350 dpi [9]. Meanwhile, the piezoelectric properties of various p-ZnO had been demonstrated. Among them, Sb-doped p-ZnO exhibited stability with a continuous span of more than 18 months [33]. Furthermore, Sb-doped p-ZnO revealed prominent piezoelectric properties in sensing and energy conversion [18,34,35]. However, these glorious works were devoid

* Corresponding author. CAS Center for Excellence in Nanoscience, Beijing Key Laboratory of Micro-nano Energy and Sensor, Beijing Institute of Nanoenergy and Nanosystems, Chinese Academy of Sciences, Beijing, 100083, PR China.
E-mail address: cfpan@binn.cas.cn (C. Pan).
[1] Zhihao Huo, Xiandi Wang and Yufei Zhang contributed equally to this work.

https://doi.org/10.1016/j.nanoen.2020.104744
Received 11 February 2020; Received in revised form 23 March 2020; Accepted 23 March 2020
Available online 2 April 2020

of in-depth exploration and analysis on the contact modes of metal-semiconductor (M-S), and the piezoelectric properties of Schottky devices with diverse structures.

Here, we synthesized the variable aspect-ratio Sb-doped ZnO nanowire (NW) films via low temperature hydrothermal method and investigated the piezotronic effect of the film through designing device structures. A Sb–ZnO/n-GaN heterostructure was demonstrated to analyze the p-type semiconducting properties of the film. And metal-insulator-semiconductor (MIS) structure was utilized to calculate the effective acceptor doping concentration, which was 5×10^{16} cm^{-3}, 1×10^{17} cm^{-3} and 2×10^{17} cm^{-3} calculated based on MIS structure with Sb/Zn atomic ratio in the solution of 0.5%, 1%, and 2%. It was also easy to obtain different contact types (Ohmic and Schottky) by contacting the Sb-doped p-ZnO NW film with metals of different work functions, which have remarkable contribution for the theoretical and practical application of p-type Schottky diodes. By investigating the piezotronic effect on the single Schottky diode and the back-to-back Schottky diode, it was found that the piezoelectric charges could modulate and tune the carriers transport at the junction. Then, a flexible self-powered strain sensor was fabricated based on the piezoelectric potential of the film, which can detect strain-relevant device performance to monitor diverse gestures motion.

2. Experimental section

2.1. Synthesis of p-ZnO nanowire films

First, a layer of 20 nm-thick ZnO seed layer was coated on PET substrates by Radio Frequency (RF) Magnetron Sputtering (PVD75 Kurt J. Lesker). The precursor solution for growing the undoped ZnO NW films consisted of 25 mM zinc nitride and 25 mM hexamethylenetetramine (HMTA). The dopant solution was prepared by mixing an equimolar ratio of sodium hydroxide (NaOH) and glycolic acid ($C_2H_4O_3$) in DI water. Then antimony acetate ($Sb(CH_3COO)_3$) is added to the precursor solution at a molar ratio of 1:12. A dopant with a concentration of 0.2% to 2% by mole relative to the Zn concentration is added to the solution. The substrate subsequently was placed in solution and reacted in an oven at 95 °C for 24 h.

2.2. Farication of the metal-insulator-semiconductor structure

As a substrate, a piece of 1 cm × 1 cm heavy doping silicon deposited by 100 nm SiO_2 in thickness was ultrasonically cleaned by alcohol, isopropyl, and deionized water in sequence, and then blew dry using argon gas. The substrate was then placed in 0.5%, 1%, 2% dopant solution, respectively, to grow NW films. Ni/Au (10 nm/40 nm) as top electrodes were finally deposited by RF Magnetron Sputtering.

2.3. Fabrication of flexible piezoelectric devices and PENGs

1% Sb-doped ZnO NW films were prepared on cleaned PET substrate directly. Gold or silver electrode was deposited through the acrylic sheet mask to obtain two piezoelectric devices with planar construction and vertical construction using Magnetron Sputtering. For PENG, Ni/Au (10 nm/40 nm) as bottom electrode was firstly deposited on the PET substrate, and then placed into precursor solutions with different doping concentrations for 4 h at 95 °C to obtain Sb–ZnO NWs film. Finally, 100-nm-thickness ITO was deposited as the top electrode.

2.4. Characterizations and measurements

The crystallization of films was characterized by X-ray Diffraction (X'Pert 3 Powder) *θ-2θ* scan with Cu-Kα radiation source. The morphology and the elemental components of the samples were investigated using Field-Emission Scanning Electron Microscopy (FESEM) (Hitachi SU8020) equipped with Energy Dispersive X-Ray Spectroscopy (EDX) (IXRF SDD2830–300D). The room-temperature photoluminescence (PL) was carried out under the excitation of a He–Cd laser (325 nm) (LabRAM HR Evolution). Electrical properties were measured via a high-impedance electrometer (Keithley 6514), Keithley 4200SCS, a probe station (Semiprobe M-6) and a customized multichannel data acquisition system (National Instruments, PXIe-4300).

3. Results and discussion

Firstly, to prepare and obtain p-ZnO films is the key challenge for the research of their piezotronic effect in this work. In fact, ZnO originally exhibits n-type semiconducting nature due to self-compensating effect of donor defects such as oxygen vacancies (V_O) and zinc gaps (Zn_i) in the host lattice [36,37]. Considerable efforts remain to implement suitable p-type dopant with high electronegativity and high solubility, and to synthesize p-ZnO nanomaterials with broad stability and low resistance. Theoretically, group-I elements as p-type dopants in ZnO are far superior to group-V elements, but the doping efficiency of the group-I elements is limited by the formation of the compensation gap [35]. Recently, As or Sb as p-type dopants have been considered to be highly promising candidates compared with N–ZnO and P–ZnO even if its atomic radius is much larger. It also predicted the possibility of forming p-type ZnO by large-size-mismatched impurity to Sb doping through first-principle calculations via Sb_{Zn}–$2V_{Zn}$ complexes model [38]. Here, Sb-doped ZnO NW films with single crystal were synthesized using low temperature solution method. The wurtzite crystal structure schematic diagram of the film is shown clearly in Fig. 1a, Zn atom is replaced by Sb atom (SbZn) in ZnO lattice. Generally, the wurtzite structure of ZnO is a hexagonal cell and a non-centrosymmetric structure. Each Zinc atom is located in a tetrahedral gap formed by four adjacent oxygen atoms. Considering the great difference in ion radius between Sb and O, Zn atom would be substituted by Sb atom, resulting in the generation of the zinc vacancy (V_{Zn}), which attract adjacent valence electrons to form a strong negative charge center.

Phase constituents and microstructure were then investigated for the controllable growth of p-ZnO NW films. The X-ray powder diffraction (XRD) patterns of as-synthesized films with different doping concentration are presented in Fig. 1b, confirming that the samples are well-crystallized hexagonal wurtzite-type ZnO (JCPDS 36–1451). Only a predominant diffraction peak corresponding to (002) crystal plane of ZnO was detected, revealing that all films have a preferred crystal growth orientation along *c*-axis perpendicular to surface of polyethylene terephthalate (PET) substrate. It was also found that full width at half maximum (FWHM) decreased when Sb/Zn molar ratio in precursor solution increased from 0% to 2%, illustrating that the crystallinity of ZnO is gradually increased (Table 1, Supporting Information). No other diffraction peaks of antimony compounds or other impurity were found within the detection limit of XRD pattern. In addition, the normalized room temperature photoluminescence (PL) spectrum of the film was observed under 325 nm continuous excitation, as shown in Fig. 1c. The defect peak (at about 560 nm) induced by oxygen vacancy (V_O) decreased with the doping concentration increasing. Then, elementary composition analysis of 2% Sb doping solution ZnO NW films was carried out using Energy Dispersive Spectrum (EDS) to further study the influence of doping concentration on growth, and only the peaks of Zn and O were observed in EDS (Fig. 1d). Furthermore, it was found that O/Zn ratio of undoped samples is 0.85 while that of 0.5% Sb-doping sample is 1.003, which is distinct for successful Sb doping (Fig. 1e). For well-grown p-type ZnO films, obviously, the doping concentration and temperature have a great impact on growth process. The morphology of films with different doping concentration were characterized by Scanning Electron Microscope (SEM), as demonstrated in Fig. 1f, depicting that the density of the nanowires gradually increases with increasing Sb doping concentration. Fig. 1g–h also show the variation in diameter and length of ZnO NW films. It can be found that the density of NWs gradually increased with doping concentration and temperature increasing,

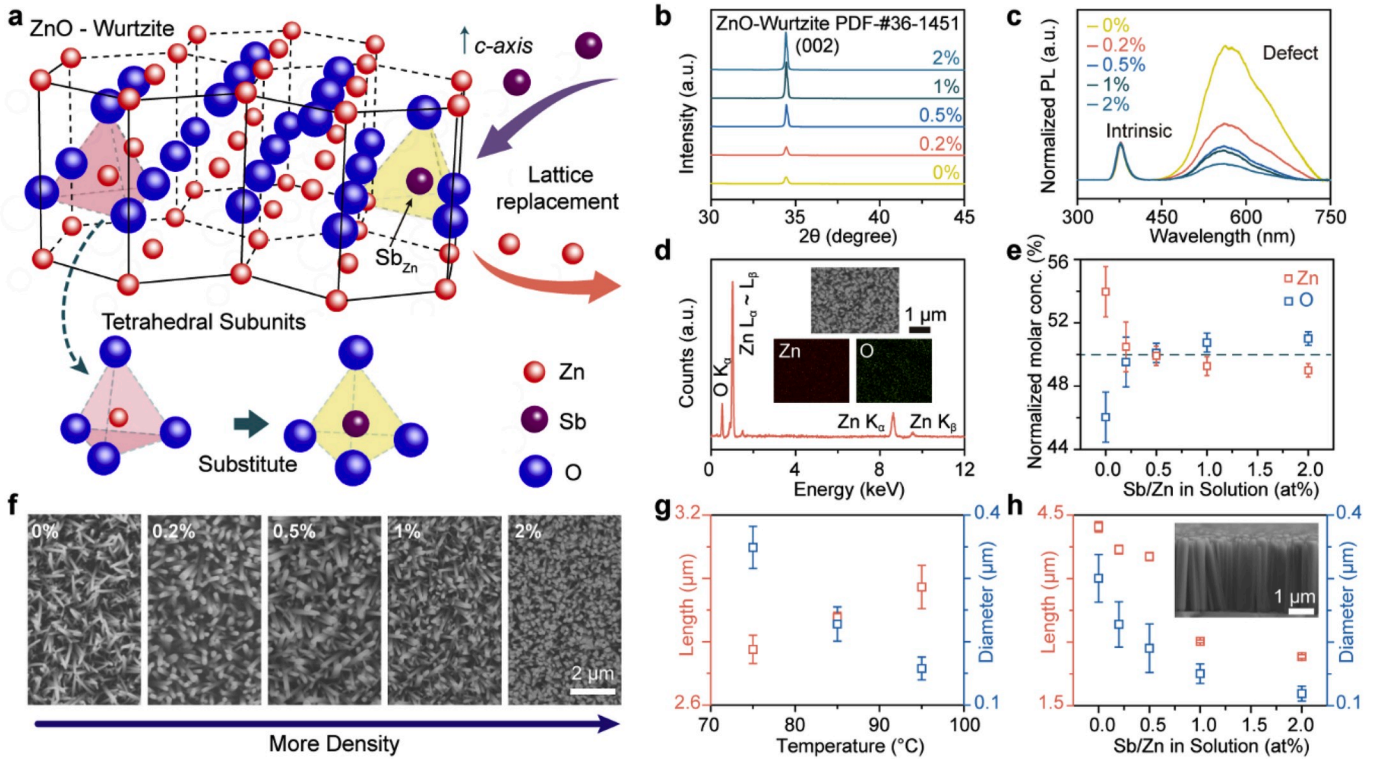

Fig. 1. Doping principle and characterization of the ZnO:Sb NW films. a) Schematic of the doped ZnO crystal structure. b) XRD pattern of ZnO films with different doping concentrations, demonstrating a typical wurtzite structure (JCPDS no. 36–1451). c) The room-temperature PL spectrum of ZnO NW films with different doping concentration under the excitation of a continuous 325 nm laser. d) EDS of the diverse samples. e) The ratio of Zn/O at different doping concentrations under EDS (97.5% confidence interval). f) SEM images of ZnO NW film with different doping concentration. g) Plot of NWs length and diameter as function of temperature at 1% Sb-doped ZnO NW films (97.5% confidence interval). h) Plot of NWs length and diameter as function of doping level at 95 °C (97.5% confidence interval).

while the length and diameter of NWs presents negative growth with doping concentration increased. The length of NWs increased positively, and inversely the diameter decreased with temperature rising. In a word, the controlled growth of Sb–ZnO NWs can be achieved by modifying the preparation parameters through the low temperature solution method, and oxygen defects gradually decreased when the increase of Sb/Zn atomic molar ratio in solution was confirmed, indicating that Sb replaces Zn and the production of V_{Zn}.

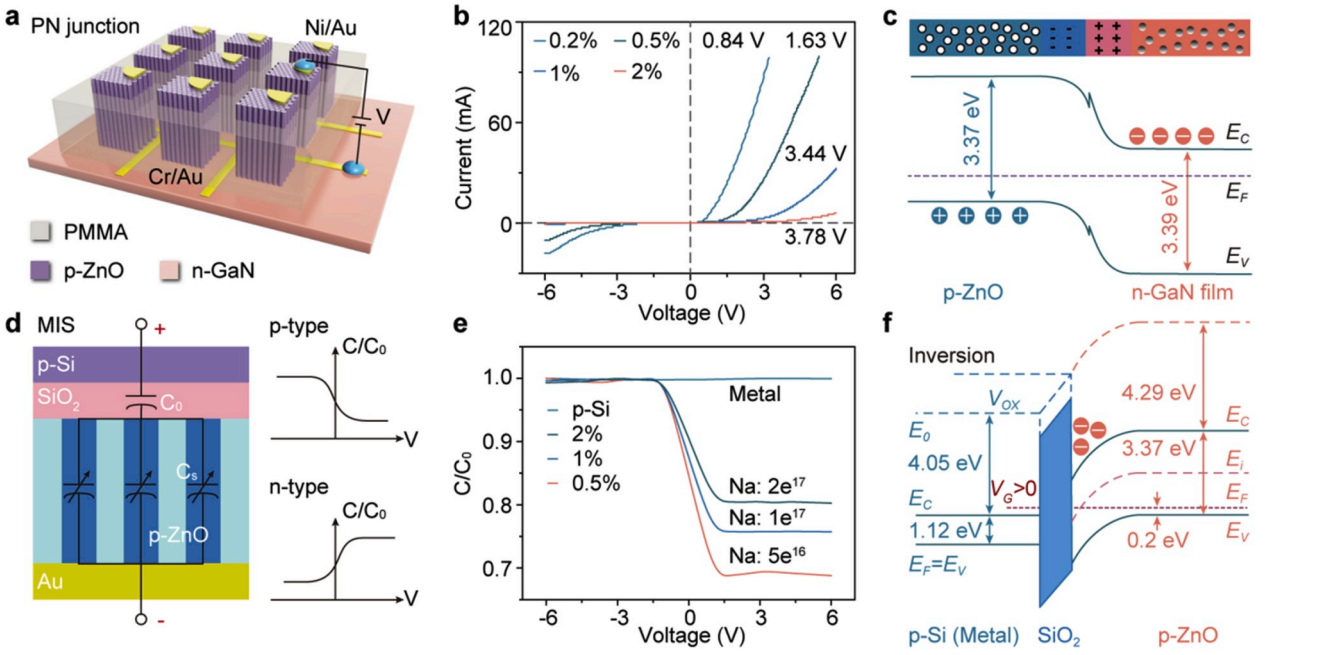

Fig. 2. The electrical properties of n-GaN/p-ZnO and the quantitative analysis of doping concentration based on MIS structure. a) Schematic illustration of the structures of the n-GaN/p-ZnO heterojunction. b) *I–V* curves of the different doping concentrations of Sb-doped ZnO/n-GaN. c) An "ideal" heterojunction energy band diagram for p-ZnO/n-GaN. d) Structure and Schematic of MIS. e) *C–V* characteristic curves of the MIS devices. f) Schematic illustration of band diagram of the MIS.

The electrical properties of as-synthesized films were demonstrated subsequently based on p-n junction. Fig. 2a presented the structure diagram of 3 × 3 pixelated arrays with Sb–ZnO/n-GaN heterostructure. The array is configurated by wet etching (5% hydrochloric acid solution) and photolithography (Fig. S1). Following this procedure, we fabricated four different heterojunction devices and exploited their electrical properties (Fig. S2 and Fig. S3). It was found that the devices with n-GaN/Sb–ZnO, p-GaN/n-ZnO exhibited excellent rectifying properties, which manifest that Sb–ZnO NW films has p-type semiconducting properties. Fig. 2b depicted the current-voltage (*I–V*) characteristic curves of Sb–ZnO/n-GaN heterostructures, which exhibit excellent rectification characteristics. As seen, the threshold voltage of p-n junction devices increases gradually with the doping concentration increasing. This is due to the higher the doping concentration of ZnO NW films, the greater contact potential difference formed with GaN film. The bandgap of ZnO and GaN at room temperature are separately assumed to be 3.37 eV and 3.39 eV [39], which construct an "ideal" heterojunction energy band diagram for p-ZnO/n-GaN according to the Anderson model. Electrons and holes will accumulate at the interface due to conduction and valence band shifting which is described in Fig. 2c. Based on the as-mentioned results, Sb–ZnO NWs are typically p-type semiconductor.

Quantitative analysis of Sb doping concentration was further explored via the capacitance-voltage (*C–V*) curves of MIS structure. The equivalent circuit diagram of MIS consisting of heavily doped p-Si, SiO_2 and p-ZnO NW films is exhibited in Fig. 2d, which is simple and easily operated. For an ideal MIS junction, its capacitance is equivalent to the overlaying capacitance of the insulation layer and the semiconductor depletion layer. Furthermore, strong inversion layer with minority carrier (electrons) will be formed at the surface of the semiconductor when a specific positive voltage is applied to the metal terminal. In fact, the width of the depletion layer will maintain a maximum value under high-frequency signal, because the rate of the generation and recombination between electrons and holes in the inversion layer cannot keep up with the change of high-frequency signal. Therefore, the capacitance of the depletion region reaches minimum value and remains constant. The corresponding *C–V* curves is schematically indicated in the upper right diagram of Fig. 2d, and it can be explained by the formula

$$\frac{C_{\min}}{C_0}=\frac{1}{1+\frac{2\varepsilon_{r0}}{\varepsilon_{rs}d_0q}\left[\frac{\varepsilon_{rs}\varepsilon_0k_0T}{N_A}\ln\left(\frac{N_A}{n_i}\right)\right]^{\frac{1}{2}}} \quad (1)$$

where n_i is the carrier concentration of the intrinsic semiconductor, N_A is the impurity concentration of the semiconductor surface (Fig. S4). In our experiments, we first tested the *C–V* characteristic of the device with the heavily doped p-Si, SiO_2, and Al, and found that the heavily doped p-Si can be served as metal gate due to the constant capacitance at different voltages under high-frequency signal. Subsequently, *C–V* curves of MIS structures at different doping concentrations were investigated, as shown in Fig. 2e. The actual acceptor carrier concentrations were calculated to be 5×10^{16} cm^{-3}, 1×10^{17} cm^{-3} and 2×10^{17} cm^{-3} corresponding to the Sb/Zn molar ratio of 0.5%, 1% and 2% in solution (Fig. S4). It must be mentioned that the preparation of insulation layer is the key and challenge for the successful implementation of the device. Fig. 2f shows the energy band diagram of the MIS structure at higher positive voltage imposed on metal. By applying sufficiently large positive bias voltage, there will be more negative charge in the MIS structure, so that the band at the interface will further bent. Hence, the intrinsic Fermi level (E_i) at the interface can be lower than the Fermi level (E_F) in semiconductor, which means the conduction band is closer to E_F than valence band. In this case, an electron inversion layer is then formed at the interface. In conclusion, we quantitatively analyzed the carrier concentration of the film using MIS structures and found that the doping concentration of these p-ZnO NW films synthesized though the low temperature solution method is approximately 10^{17} cm^{-3}.

Fortunately, the as-synthesized p-ZnO film was beneficial to the controllability of the M-S contact mode, which is of great significance to the development of p-type Schottky diodes. Actually, the surface state density of semiconductor is quite high and close to one-third of the bandgap from the valence-band edge, resulting in the clamp effect of the Schottky barrier height (SBH) [40]. Therefore, it is easier to form Ohmic contact for p-type semiconductor, and to form Schottky contact for n-type semiconductor. In addition, some studies have also found that the surface state has less influence on the SBH of certain semiconductors (e.g., AlN, ZnO, InA_S) [41]. Nevertheless, n-ZnO fabricated using solution method generally has a large amount of oxygen defects, resulting in the enhancement of the pinning effect. In this work, as-synthesized p-ZnO NW film has less oxygen vacancy, thus we assumed that the corresponding SBH will be affected by the metal electrodes. The *I–V* characteristic curves of the device constructed by Sb-doped ZnO NW films and metal with different work functions (Ag/Au) were obtained, as depicted in Fig. 3a. It is clearly verified that the device exhibits Ohmic contact when both electrodes are Au, and shows the single Schottky contact when one electrode is Au and the other is Ag, and presents two back-to-back Schottky barriers when both electrodes are Ag. Noteworthy, the voltage drop occurs at the reversely biased Schottky barrier, so that the order of magnitude of current for two back-to-back Schottky barriers model is significantly less than the other two models. Thus, we infer that the M-S contact mode between p-ZnO NW films and the metal is more controllable. Commonly, it will be Ohmic contact through depositing Au electrode and Schottky contact via applying Ag electrode.

The piezotronic effect on p-ZnO NW films with single Schottky junction was studied. In this work, p-ZnO NW films with 1% Sb doping concentration was employed, which grow along the *c*-axis direction on the PET substrate [33,42]. The thickness of PET is prominently larger than that of film, so it can be assumed that the film will be subjected to tensile strain parallel to the substrate surface when it is bent downward, whereas it will be subjected to compressive strain under bent upward. Moreover, the piezoelectric potential distribution of the film under deformation was simulated using commercial finite element analysis method (COMSOL) (Fig. S5). It was found that the upper surface of the film would generate negative piezoelectric charges under tensile strain and induce positive piezoelectric charges upon compression strain. To investigate the effect of piezoelectric charges on carrier transport characteristics, two different Schottky device structures (vertical structure and planar structure) were designed, and their *I–V* characteristic curves under strain were measured using Ag electrodes at both ends of the injection, as shown in Fig. 3b–c. It can be observed that the Schottky diode is turn-on under negative bias and cut-off at applied positive bias. Furthermore, for devices with planar structures under negative bias voltage, the currents increase with increasing compressive strain and decrease with tensile strain rising, vice versa under positive bias voltage, as demonstrated in Fig. 3b. And Schottky barrier height ($\Delta\Phi_S$) reduced under tension strain and enhanced under compressive strain at 2 V (more information is shown in Fig. S6). On the other hand, for devices with the vertical structure under negative bias, the currents exhibit a strengthening trend under tensile strain increasing and a decreasing trend with compressive strain increasing (Fig. 3c), but the $\Delta\Phi_S$ increased under tension strain and decreased under compressive strain at 2 V. In fact, not only the piezoelectric effect but also the piezoresistive effect will lead to the change in SBH and then tune carrier transportation under applied strain. The change in current is the same under different voltages for piezoresistive effect (Fig. S7). However, the experimental results revealed that the variation trend of the current was inverse under the polarity of voltage after applied strain and the corresponding variation trend of SBH was inconsistent for two different device structures, which indicated that carrier transport was dominated by piezoelectric effect rather than piezoresistance effect. To further understand the strain-induced piezoelectric effect, the charge field distribution in the contact region under thermal equilibrium is systematically analyzed, as shown in Fig. 3d. When the metal contacts with the film, holes in p-ZnO

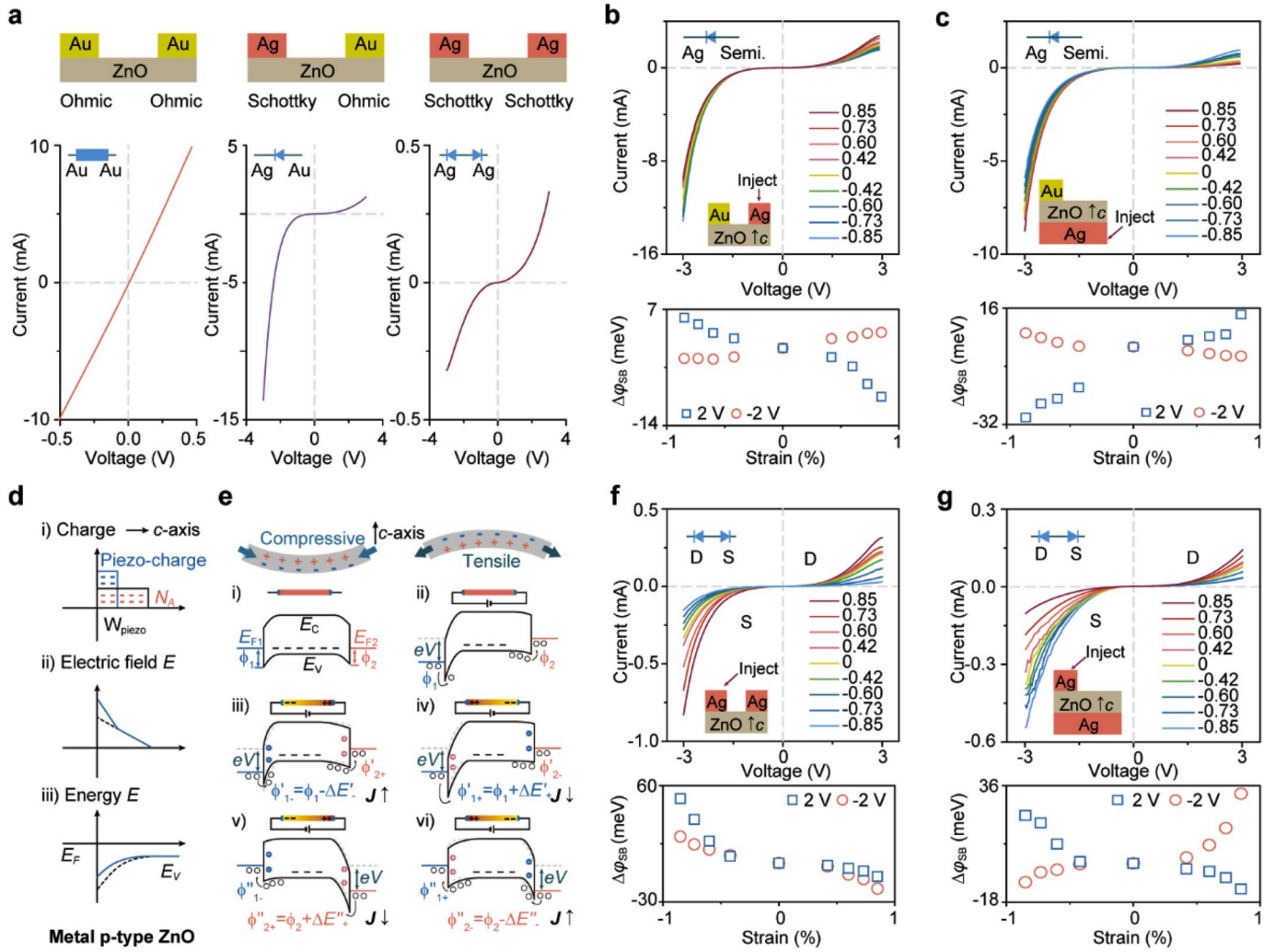

Fig. 3. Piezoelectric effects of different structures in 1% Sb-doped p-ZnO NW films. a) *I–V* characteristics cuvers and simple structure diagram of p-ZnO NW films in contact with Ag or Au. In the singal-Schottky sample, *I–V* characteristics curves of the two different structures (planar and vertical electrode structures) as a function of strain and the variation of SBH are demonstrated in b) and c), respectively. The ideal Schottky contact, when the junction is piezoelectrically charged and in thermal equilibrium: di) Space charge distribution. dii) Electric field distribution. diii) Energy band diagram without (black dash line) and with (blue solid line) piezoelectric charge externally due to applied strain. e) Schematic band diagrams of Schottky devices based on p-ZnO NW film and metal electrode. *I–V* characteristics of the two different structures as function of the strain and the variation of SBH are demonstrated in f) and g) for two back-to-back Schottky device, respectively.

films will flow toward the metal if the work function of metal is smaller than that of semiconductor, resulting in the generation of the Schottky barrier at interface. And the piezoelectric polarized charges are induced at the interface by applied strain. Taking the negative piezoelectric charge as an example, it will further increase the electric field at the interface and lower the SBH, eventually leading to the enhancement of the current density (Fig. 3d). For our devices, the opposite piezoelectric charges are induced at the junction for the two different device structures under the same strain, resulting in the asymmetry of the current characteristics. Obviously, the influence of piezoelectric charge on the carrier transport properties in Schottky junction was verified through different structural designs. In other word, the negative piezoelectric charge reduces SBH and increases the current, while positive piezoelectric charge causes an increment in SBH and induced a decline in the current.

The piezotronic effect on p-ZnO NW films with two back-to-back Schottky contacts was further studied. Based on *I–V* curve in Fig. 3a–iii, the two back-to-back Schottky diodes would be built in which the p-ZnO NW film connected with two Ag electrodes. We defined the Ag electrode at the injection end as the drain and the other as the source. The voltage drop occurs mainly at the reversely biased Schottky barrier at the source side when a negative voltage is applied to the drain. Fig. 3e (i-ii) introduced the band structure of the devices under equilibrium conditions and in condition of the drain positive. According to the above-mentioned analysis of single Schottky samples, different piezoelectric charges are created on the upper and lower surfaces of the film when strain occurs, which can thereby tune/control charge carrier transportation. Assuming that the negative piezoelectric charge is induced at drain and the positive charge is formed on source contact with the drain positive bias (Fig. 3e–iii), the negative piezoelectric charge at the drain lowers SBH and gives rise to more holes moving from the semiconductor into the metal, which brings an enhancement on the current. Meanwhile, the effect of the positive piezoelectric charge on the current is negligible due to the forward bias of Schottky barrier at the source side. Similarly, the current will decrease with SBH increasing when the positive piezoelectric charge is induced on the reversely biased at the drain side (Fig. 3e–iv). Therefore, we conclude that charge carrier transport characteristics are mainly controlled by the variation of SBH in the reversely biased state. Fig. 3e(v-vi) also exhibits the effect of the piezoelectric charge on the energy band structure in the reversely biased

Schottky junction state at the source side. To further verify this theory, two device structures were constructed. For the device with the planar structure, the induced piezoelectric charges are the same when the source or the drain is in reversely biased state. In contrast, the polarity of piezoelectric charge is different for the device for the vertical structure. As shown in Fig. 3f, the current augments with tensile strain increasing while reducing with compressive strain upward when the source or the drain is in reversely biased state, and the corresponding SBH fluctuates uniformly. However, the corresponding fluctuation of *I–V* curves were different for devices with vertical structures, the current diminished in accompany with tensile strain rising (at the reversely biased source side) under negative bias but the current increased under positive bias (at the reversely biased drain side), as shown in Fig. 3g. The reason is that the piezoelectric effect has an asymmetrical effect on the source and drain due to the diversity in the polarity of the piezoelectric potential.

PENGs were further fabricated via the Schottky devices with vertical structure constructed by the ITO electrode and Sb-doped p-ZnO films. PENGs were first confirmed by Schottky behavior test (Fig. S8), switching polarity tests and a linear superposition [15]. The short-circuit currents of different PENGs were then periodically stretched and released at a strain of 0.88%, as demonstrated in Fig. 4a. Regardless of the devices A or B, the positive output current came out when the device was stretched, and the negative output current was produced when released. The relevant polarity inversion tests were shown in Fig. 4a–ii and Fig. 4a–iv. Devices A and B are then connected in parallel and anti-parallel to examine the linear superposition of current. It could be found that the output current was the sum of their individual output current when the two PENGs are connected in the same direction (Fig. 4a–v), and the output current is the difference of their individual output current when connected in reverse direction (Fig. 4a–vi). According to the performance of device obtained by the test, it is determined that the output signal of PENGs is real.

Self-powered strain sensors with the p-ZnO NW films were then explored. Distinctly, external strain and doping concentration have a

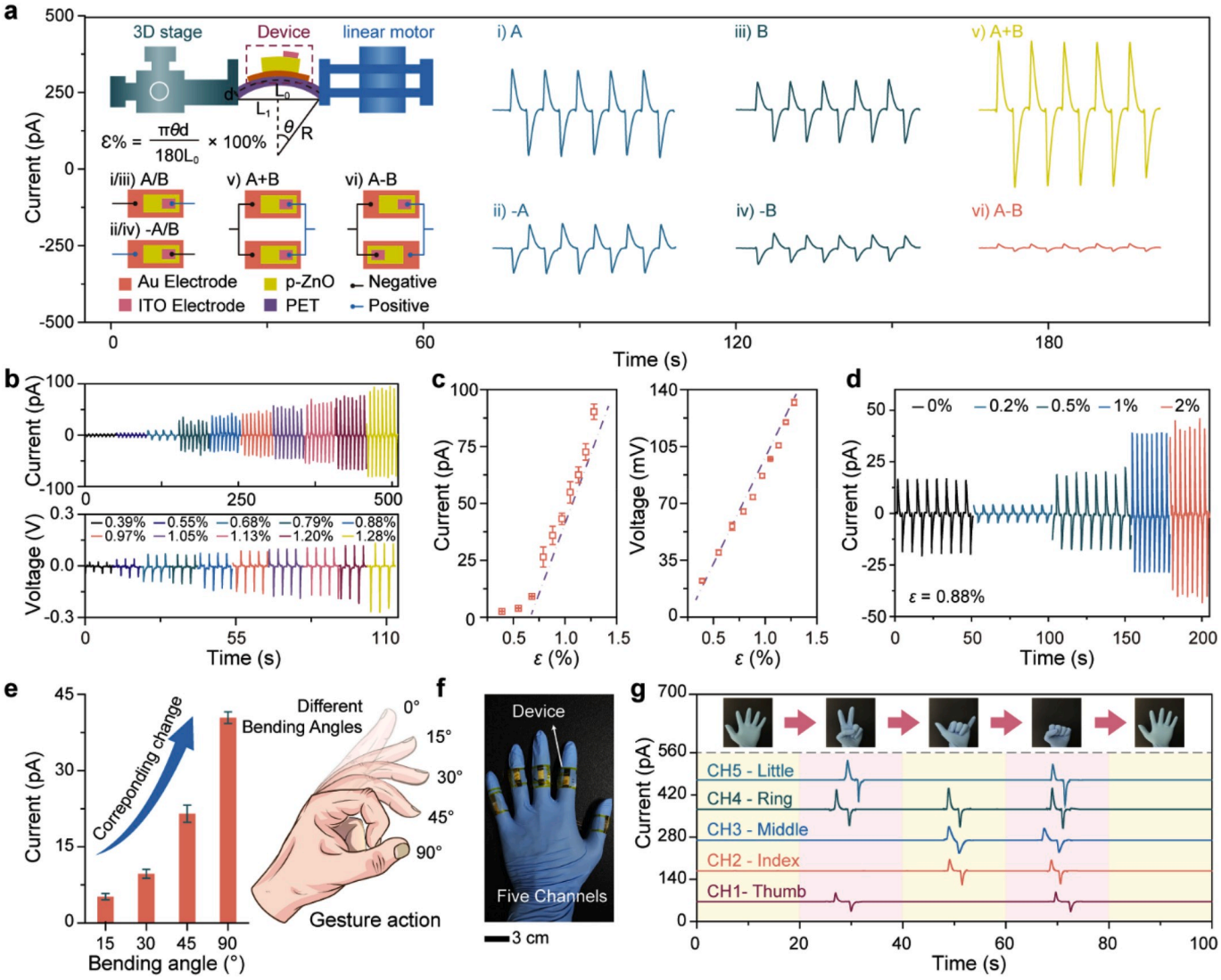

Fig. 4. Electrical output of flexible PENGs and strain sensors by utilizing p-type ZnO NW films. a) The short-circuit current of devices A, B under the strain of 0.88% measured in the forward connections (ai) and (aiii), respectively. aii,aiv) The short-circuit output current when devices A and B are reverse connected. av,avi) The properties of output current when devices A and B are connected in parallel and anti-parallel. The corresponding connection configuration of the two devices in reference to the measurement system illustrated in the left of (a). b) Open-circuit output voltage and short-circuit current power output of 2% Sb doping p-ZnO NWs film under different strain. c) The corresponding changes of maximum voltage and current with strain (97.5% confidence interval). d) Short-circuit current power output of different doping p-ZnO NWs film under a strain of 0.88%. e) Schematic diagram of gesture action and the output property of the device is measured as a function of the index finger flexion difference degrees of curvature (97.5% confidence interval). f) Photograph of the devices bound to five fingers is constructed into a multi-channel system. g) Testing multiple gestures with a multi-channel system has demonstrated the ability of the device to detect complex gesture motion.

significant effect on the performance of strain sensors. The open-circuit voltage and short-circuit current of the sensor (2% doped) were measured (Fig. 4b), dipicting that the output is significantly improved with increased strain. The maximum voltage output and current output have a positive correlation with the applied strain, as shown in Fig. 4c. Furthermore, the sensor has well durability and excellent stability in a repeatedly stretching-releasing state at a deformation frequency of 0.33 Hz under 0.88% (Fig. S9). In addition, the corresponding output current of samples with different doping levels at a constant strain of 0.88% was presented in Fig. 4d. Although the previous theory insists that the doping concentration has a certain shielding effect on the piezoelectric effect [43,44], the piezoelectric effect is affected by the doping concentration, the change of the nanowire diameter and the degree of bending of the sample, which explains the output performance of our devices exhibits a trend of decreasing first and then increasing. To obtain better signal-to-noise ratio, 2% Sb-doped p-ZnO NW films is selected to construct strain sensors that perceive and respond to the gesture movement. The electrical signals of one single device at different bending points of the index finger was obtained and summarized in Fig. 4e. The output current was positively correlated with the bending degree of finger. Multiple-finger-motion-driven electrical signals were then simulated by multi-channel data acquisition systems to exhibit gesture movement, as presented in Fig. 4f. The sensor can not only detect the motion of each finger individually and accurately, but also evaluate change in gestures based on the output signal. Our devices are light-weight, easy to synthesize, and low-cost, which provides potential possibility in applications, for instance, flexible electronic devices, wearable devices, robotics and health care.

4. Conclusion

In summary, we explored the piezotronic effect of self-powered piezoelectric strain sensors constructed by a series of various sizes Sb-doped p-ZnO NW films. The film was fabricated via low temperature hydrothermal method. The actual doping concentration was approximately 10^{-17} cm^{-3} by measuring the *C–V* characteristics of MIS structure. It was also found that the p-ZnO film was beneficial for the controllability of the MS contact mode. By designing two different device structures, the piezotronic effect on single Schottky junction diodes and two back-to-back Schottky diodes was systematically investigated. The negative piezoelectric charge can reduce SBH and enhance the current while positive piezoelectric charge stimulates a decline in the current. In addition, self-powered strain sensors that can convert mechanical energy into electrical energy were manufactured using p-ZnO PENGs, which not only work stably and independently, but also clearly show the change of the gesture. We believe that the device has potential practical applications in intelligent robots, wearable electronic devices, and medical monitoring systems.

Declaration of competing interest

The authors declare that they have no known competing financial interests or personal relationships that could have appeared to influence the work reported in this paper.

CRediT authorship contribution statement

Zhihao Huo: Writing - review & editing, Writing - original draft, Investigation, Formal analysis, Methodology, Software. **Xiandi Wang:** Data curation, Software, Writing - review & editing, Visualization. **Yufei Zhang:** Writing - review & editing. **Bensong Wan:** Validation. **Wenqiang Wu:** Methodology. **Zheng Yang:** Software. **Guofeng Hu:** Conceptualization. **Xiangyu Li:** Investigation. **Caofeng Pan:** Project administration, Resources, Supervision, Validation, Funding acquisition.

Acknowledgements

The authors express thanks for the support of Natural Science Foundation of Beijing Municipality (2184131, 4181004, 4182080, 4184110, and Z180011), national key R & D project from Minister of Science and Technology, China (2016YFA0202703), National Natural Science Foundation of China (Nos. 61804011, 51622205, 61675027, 51432005, 61505010, 51502018), Beijing City Committee of science and technology (Z171100002017019 and Z181100004418004), and the University of Chinese Academy of Sciences.

Appendix A. Supplementary data

Supplementary data to this article can be found online at https://doi.org/10.1016/j.nanoen.2020.104744.

References

[1] C. Pan, J. Zhai, Z.L. Wang, Chem. Rev. 119 (2019) 9303–9359.
[2] Q. Hua, J. Sun, H. Liu, R. Bao, R. Yu, J. Zhai, C. Pan, Z.L. Wang, Nat. Commun. 9 (2018) 244.
[3] Z.L. Wang, W. Wu, C. Falconi, MRS Bull. 43 (2018) 922–927.
[4] S. Qiao, J. Liu, G. Fu, K. Ren, Z. Li, S. Wang, C. Pan, Nano Energy 49 (2018) 508–514.
[5] G. Hu, W. Guo, R. Yu, X. Yang, R. Zhou, C. Pan, Z.L. Wang, Nano Energy 23 (2016) 27–33.
[6] M. Law, L.E. Greene, J.C. Johnson, R. Saykally, P.D. Yang, Nat. Mater. 4 (2005) 455–459.
[7] C. Pan, M. Chen, R. Yu, Q. Yang, Y. Hu, Y. Zhang, Z.L. Wang, Adv. Mater. 28 (2016) 1535–1552.
[8] C. Wang, R. Ba, K. Zhao, T. Zhang, L. Dong, C. Pan, Nano Energy 14 (2015) 364–371.
[9] C. Pan, L. Dong, G. Zhu, S. Niu, R. Yu, Q. Yang, Y. Liu, Z.L. Wang, Nat. Photon. 7 (2013) 752–758.
[10] X. Wang, D. Peng, B. Huang, C. Pan, Z.L. Wang, Nano Energy 55 (2019) 389–400.
[11] J. Zhou, Y.D. Gu, P. Fei, W.J. Mai, Y.F. Gao, R.S. Yang, G. Bao, Z.L. Wang, Nano Lett. 8 (2008) 3035–3040.
[12] C. Wang, J. Zhao, C. Ma, J. Sun, L. Tian, X. Li, F. Li, X. Han, C. Liu, C. Shen, L. Dong, J. Yang, C. Pan, Nano Energy 34 (2017) 578–585.
[13] Z.L. Wang, Adv. Mater. 24 (2012) 4632–4646.
[14] Z.L. Wang, Nano Today 5 (2010) 540–552.
[15] R. Yang, Y. Qin, L. Dai, Z.L. Wang, Nat. Nanotechnol. 4 (2008) 34.
[16] Z.L. Wang, J.H. Song, Science 312 (2006) 242–246.
[17] J. Sun, X. Pu, C. Jiang, C. Du, M. Liu, Y. Zhang, Z. Liu, J. Zhai, W. Hu, Z.L. Wang, Sci. Bull. 63 (2018) 795–801.
[18] K.C. Pradel, W. Wu, Y. Ding, Z.L. Wang, Nano Lett. 14 (2014) 6897–6905.
[19] S. Xu, Y. Qin, C. Xu, Y. Wei, R. Yang, Z.L. Wang, Nat. Nanotechnol. 5 (2010) 366–373.
[20] D. You, C. Xu, F. Qin, Z. Zhu, A.G. Manohari, W. Xu, J. Zhao, W. Liu, Sci. Bull. 63 (2018) 38–45.
[21] X. Ren, X. Zhang, N. Liu, L. Wen, L. Ding, Z. Ma, J. Su, L. Li, J. Han, Y. Gao, Adv. Funct. Mater. 25 (2015) 2182–2188.
[22] J.C. Fan, K.M. Sreekanth, Z. Xie, S.L. Chang, K.V. Rao, Prog. Mater. Sci. 58 (2013) 874–985.
[23] M.P. Lu, J. Song, M.Y. Lu, M.T. Chen, Y. Gao, L.J. Chen, Z.L. Wang, Nano Lett. 9 (2009) 1223–1227.
[24] Z.L. Wang, Adv. Mater. 19 (2007) 889–892.
[25] Z.H. Huo, Y.Y. Peng, Y.F. Zhang, G.Y. Gao, B.S. Wan, W.Q. Wu, Z. Yang, X. D. Wang, C.F. Pan, Adv. Mater. Interfaces. 5 (2018) 1801061.
[26] W. Wu, X. Wen, Z.L. Wang, Science 340 (2013) 952–957.
[27] W. Wu, Y. Wei, Z.L. Wang, Adv. Mater. 22 (2010), 4711-+.
[28] R. Zhou, G. Hu, R. Yu, C. Pan, Z.L. Wang, Nano Energy 12 (2015) 588–596.
[29] G. Hu, R. Zhou, R. Yu, L. Dong, C. Pan, Z.L. Wang, Nano Res. 7 (2014) 1083–1091.
[30] X.D. Wang, Y.F. Zhang, X.J. Zhang, Z.H. Huo, X.Y. Li, M.L. Que, Z.C. Peng, H. Wang, C.F. Pan, Adv. Mater. 30 (2018) 1706738.
[31] S. Huang, G. Tang, H. Huang, X.-g. Wu, P. Zhou, L. Zou, L. Xie, J. Deng, X. Wang, H. Zhong, J. Hong, Sci. Bull. 63 (2018) 1254–1259.
[32] W. Guo, X. Li, M. Chen, L. Xu, L. Dong, X. Cao, W. Tang, J. Zhu, C. Lin, C. Pan, Z. L. Wang, Adv. Funct. Mater. 24 (2014) 6691–6699.
[33] F. Wang, J.H. Seo, D. Bayerl, J. Shi, H. Mi, Z. Ma, D. Zhao, Y. Shuai, W. Zhou, X. Wang, Nanotechnology 22 (2011) 225602.
[34] C. Cao, X. Xie, Y. Zeng, S. Shi, G. Wang, L. Yang, C. Wang, S. Lin, Nano Energy 61 (2019) 550–558.
[35] K.C. Pradel, W.Z. Wu, Y.S. Zhou, X.N. Wen, Y. Ding, Z.L. Wang, Nano Lett. 13 (2013) 2647–2653.
[36] U. Ozgur, Y.I. Alivov, C. Liu, A. Teke, M.A. Reshchikov, S. Dogan, V. Avrutin, S. J. Cho, H. Morkoc, J. Appl. Phys. 98 (2005).
[37] H. Zeng, G. Duan, Y. Li, S. Yang, X. Xu, W. Cai, Adv. Funct. Mater. 20 (2010) 561–572.
[38] S. Limpijumnong, S.B. Zhang, S.H. Wei, C.H. Park, Phys. Rev. Lett. 92 (2004).

[39] D.K. Hwang, S.H. Kang, J.H. Lim, E.J. Yang, J.Y. Oh, J.H. Yang, S.J. Park, Appl. Phys. Lett. 86 (2005).
[40] C. Mead, W. Spitzer, Phys. Rev. Lett. 10 (1963) 471.
[41] C.A. Mead, Solid State Electron. 9 (1966) 1023–1033.
[42] B. Liu, H.C. Zeng, J. Am. Chem. Soc. 125 (2003) 4430–4431.
[43] G. Mantini, Y.F. Gao, A. D'Amico, C. Falconi, Z.L. Wang, Nano Res. 2 (2009) 624–629.
[44] J. Zhou, P. Fei, Y. Gu, W. Mai, Y. Gao, R. Yang, G. Bao, Z.L. Wang, Nano Lett. 8 (2008) 3973–3977.

Zhihao Huo received his undergraduate degree from the University of Jinan in 2016. Currently he is pursuing his PhD under the supervision of Prof. Caofeng Pan at Beijing Institute of Nanoenergy and Nanosystems, Chinese Academy of Sciences. His current research interests focus on low-dimensional piezoelectric semiconductor micro/nanophotoelectric function device.

Xiandi Wang received his PhD degree in condensed matter physics from the University of Chinese Academy of Sciences in 2016. He had been a postdoc fellow in the group of Professor Zhong Lin Wang at National Center for Nanoscience and Technology. Now he has been an associate professor in the group of Prof. Caofeng Pan at Beijing Institute of Nanoenergy and Nanosystems, CAS since 2018. His research interests mainly focus on the fields of piezo-photonic effect and triboelectric nanogenerator for fabricating novel flexible large-scale tactile sensor matrix and stretchable electronics.

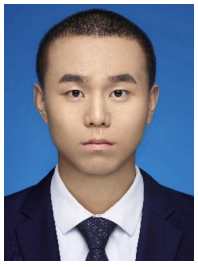

Yufei Zhang received his master's degree in Materials Science & Engineering from Beihang University in 2019. He is currently a Ph. D. Candidate majored in Nanomaterials and devices at Beijing Institute of Nanoenergy and Nanosystems, CAS. His research focuses on stretchable transparent materials and wireless wearable electronic devices.

Bensong Wan received his Bachelor's degree and Ph. D. degree from Beihang University in 2013 and 2019, respectively. He is now working as a postdoctor under the supervision of Prof. Caofeng Pan at Shenzhen University. His researches mainly focus on the synthesis of 2D materials and fabication of nano electronic devices.

Wenqiang Wu is currently a Ph.D. candidate in the College of Materials Science and Engineering, Hunan University. Since 2016, he has been a visiting student in the group of Prof. Caofeng Pan at Beijing Institute of Nanoenergy and Nanosystems, Chinese Academy of Sciences. His research focuses on the controllable synthesis of perovskite materials and the fabrication of high-performance photodetector array.

Jianguo Xi received his B. S. Degree (2010) from Taiyuan University of Science and Technoloygy, and then graduated from China University of Geosciences as a Ph. D. (2015). He then joined in Auburn University as a postdoctoral fellow. He is currently a joint postdoctor of Dr. Wenjie Mai's group at Jinan University and Dr. Canfeng Pan's group at Beijing Institute of Nanoenergy and Nanosystem since 2019. His main research interests focus on the fields of 2D materials for fabricating novel Van Der Waals heterostructures and the application in the piezoelectric and piezophototronic devices.

Zheng Yang received his PhD degree in Nanoscience and Nanotechnology from the Beijing Institute of Nanoenergy and Nanosystems(CAS) in 2019.Then he joined the College of Physics Science and Technology at Hebei University. His research is mainly focused on the controllable growth and optoelectronics applications of lead halide perovskites.

Guofeng Hu received his undergraduate degree from Tianjin Polytechnic University in 2010. Then, he received his PhD from Beijing Institute of Nanoenergy and Nanosystems, CAS under the supervision of Prof. Caofeng Pan in 2015. Currently, he is a post-doctoral researcher at Shenzhen University. His research is mainly focused on photoelectric devices and electronic applications of piezotronics and piezophototronics based on 2D materials.

Xiangyu Li received his undergraduate degree from Nanchang University in 2017. Currently he is pursuing his M.S under the supervision of Prof. Caofeng Pan at Beijing Institute of Nanoenergy and Nanosystems, CAS. His research is mainly focused on new triboelectric nanogenerator.

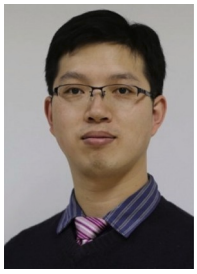

Dr. Caofeng Pan received his B.S. degree (2005) and his Ph.D. (2010) in Materials Science and Engineering from Tsinghua University, China. He then joined the Georgia Institute of Technology as a postdoctoral fellow. He is currently a professor and a group leader at Beijing Institute of Nanoenergy and Nanosystems, Chinese Academy of Sciences since 2013. His main research interests focus on the fields of piezotronics/piezo-phototronics for fabricating new electronic and opto-electronic devices, nano-power source (such as nanofuel cell, nano biofuel cell and nanogenerator), hybrid nanogenerators, and self-powered nanosystems. Details can be found at http://piezotronics.binncas.cn/index%20en.php.